applied sciences

MDPI

Article

Multifractal Characteristics of Gravel Grain Size in Riparian Zones of a Karst–Clastic Rock Composite Watershed of Southwest China: A Case Study of the Chishui River Basin

Yifei Ren *, Jihong Xia *, Wangwei Cai, Jiayi Zu, Yue Wang, Kengran Chen, Yuanshuo Lu and Yating Huang

College of Agricultural Science and Engineering, Hohai University, Nanjing 210098, China
* Correspondence: 241310010031@hhu.edu.cn (Y.R.); syjhxia@hhu.edu.cn (J.X.)

Featured Application

Image-based gravel measurements combined with conventional and multifractal descriptors may support comparative assessments of riparian sediment heterogeneity in river-corridor monitoring.

Abstract

Gravel grain-size distributions in riparian zones may exhibit substantial spatial variability in geologically heterogeneous watersheds. This study combined conventional grain-size statistics and multifractal analysis of high-resolution quadrat images from 15 mainstem and tributary sampling sites in the Chishui River Basin, Southwest China. The measured surface gravel sizes ranged from 0.07 to 141.07 cm, with pronounced site-to-site differences in grain-size composition, median grain size (D_{50}), and dispersion. No statistically significant differences in conventional grain-size descriptors were detected among the upstream, midstream, and downstream zones. Generalized-dimension spectra exhibited broadly similar inverse-S-shaped trends, while the generalized-dimension spectrum width (ΔD) and singularity-spectrum width ($\Delta\alpha$) varied among sampling sites. Singularity-spectrum asymmetry (Δf) remained negative with relatively limited variation under the selected moment-order range. Spearman correlation analysis, with Benjamini–Hochberg correction applied to 21 original comparisons, identified a significant negative association between standard deviation (SD) and ΔD ($\rho = -0.750$, adjusted $q = 0.013$). The selected relationships between D_{50} and ΔD and between the coefficient of variation and Δf were not significant after correction. These findings suggest that conventional grain-size descriptors and multifractal parameters may capture partially different aspects of the observed grain-size distributions. Given the limited and uneven spatial sampling, the results should be interpreted as site-specific observations that may provide preliminary reference information for investigations in river systems with comparable geological settings.

Keywords: gravel grain size; multifractal analysis; spatial variability; grain-size distribution; karst–clastic rock composite watershed; Chishui River Basin

Check for updates

Academic Editor: Sungchul Yang

Received: 12 October 2026
Revised: 15 November 2026
Accepted: 18 November 2026
Published: 19 November 2026

Copyright: © 2026 by the authors. Licensee MDPI, Basel, Switzerland. This article is an open access article distributed under the terms and conditions of the Creative Commons Attribution (CC BY) license.

1. Introduction

Gravel grain-size characteristics in riparian zones provide important information on sediment supply, redistribution, storage, and local depositional conditions along river corridors. These processes may be particularly complex in karst regions, where lithology strongly influences weathering, runoff generation, sediment availability, and sediment-delivery pathways. Southwest China contains one of the world's largest contiguous karst regions, but

its river basins are rarely composed exclusively of carbonate rocks. Instead, carbonate formations commonly coexist with siliciclastic rocks, shale, and mixed sedimentary strata, forming lithologically heterogeneous karst–clastic rock composite watersheds. Previous studies have shown that lithological and geomorphic differences can substantially affect sediment yield and sediment connectivity in such heterogeneous karst catchments [1–3]. Consequently, understanding how gravel grain-size distributions in riparian zones vary under this composite geological setting is important for interpreting sediment organization and spatial variability in rivers of Southwest China.

Carbonate- and clastic-rock terrains can differ substantially in both sediment production and hydrological response. Carbonate-dominated karst areas are characterized by dissolution, fissures, conduits, and strong surface–subsurface hydrological exchange, which may reduce or redistribute surface sediment transport. In contrast, clastic-rock units generally provide larger amounts of insoluble particulate material and may support more continuous surface sediment delivery. Where these lithologies coexist within the same watershed, gravel deposits in riparian zones may therefore integrate materials derived from contrasting weathering and transport pathways. Studies in heterogeneous karst catchments of Southwest China have demonstrated strong relationships between lithological composition and sediment yield, while sediment transport can also vary substantially with rainfall, hydrological connectivity, and geomorphic setting [1–3]. Such contrasts make karst–clastic rock composite watersheds particularly suitable for examining spatially complex grain-size distributions.

Gravel grain-size distributions are commonly summarized using descriptors such as D_{50}, mean grain size, standard deviation, coefficient of variation, and the proportions of different grain-size classes [4,5]. These metrics efficiently describe central tendency, bulk dispersion, and dominant grain-size composition and remain indispensable for sedimentological characterization. However, individual statistical descriptors emphasize different aspects of a distribution and do not explicitly characterize how grain-size subsets with different occurrence probabilities vary across scales. This limitation may be particularly relevant in lithologically heterogeneous karst–clastic rock composite watersheds, where contrasting sediment sources and transport pathways can produce broad, skewed grain-size distributions containing both dominant fine-to-medium fractions and low-frequency coarse particles. Consequently, samples with similar mean grain size or coefficients of variation may still differ in their internal probability structure. Combining conventional grain-size descriptors with approaches that quantify scale-dependent properties may therefore provide additional information on the internal probability structure of gravel grain-size distributions, particularly the characteristics of grain-size components occurring at different frequencies [6–8].

Multifractal analysis provides a complementary approach for characterizing scale-dependent properties of complex grain-size distributions [9–11]. Rather than reducing a distribution to a single statistic, the multifractal framework varies the statistical moment order q to emphasize subsets with different occurrence probabilities and uses generalized dimensions and singularity spectra to characterize their scale-dependent structure. Fractal and multifractal approaches have been applied to fluvial sediments and other particle-size systems [12]. For gravel deposits in riparian zones of lithologically heterogeneous karst–clastic rock composite watersheds, however, the relationships between conventional grain-size characteristics and probability-dependent scaling properties remain insufficiently characterized. In particular, the generalized-dimension spectrum width (ΔD), singularity-spectrum width ($\Delta\alpha$), and singularity-spectrum asymmetry (Δf) describe different aspects of the grain-size probability distribution, including variations in scaling behavior and spectral shape. Examining their spatial variability and statistical relationships with conventional

grain-size descriptors may help identify differences in grain-size distribution structure that are not directly expressed by measures of particle-size magnitude, composition, and dispersion. Such comparisons provide a basis for understanding the multifractal characteristics of riparian gravel deposits under heterogeneous geological conditions.

To address these questions, we investigated the Chishui River Basin in Southwest China using high-resolution quadrat imagery of surface gravel from 15 sampling sites distributed across the mainstem and tributaries. The coexistence of carbonate rocks, clastic rocks, and mixed sedimentary formations provides a geologically heterogeneous setting for examining gravel grain-size distributions in riparian zones. Grain-size information derived from the imagery was analyzed using both conventional statistical descriptors and multifractal metrics. Specifically, this study aims to: (1) characterize gravel grain-size composition and distribution among sampling sites and broad longitudinal zones; (2) examine the generalized-dimension and singularity-spectrum characteristics and their spatial variability; (3) evaluate the relationships between conventional grain-size metrics and selected multifractal descriptors to explore potential information overlap and complementarity; and (4) discuss possible environmental influences on the observed patterns within the limitations of the available field observations.

2. Materials and Methods

2.1. Study Area

The Chishui River Basin is located along the northern margin of the Yunnan–Guizhou Plateau in southwestern China, within the transition between the plateau and the Sichuan Basin (104°45′–106°51′ E, 27°20′–28°50′ N). The Chishui River is a first-order tributary entering the upper Yangtze River from the right bank. It originates in Zhenxiong County, Yunnan Province, flows generally northeastward along the Guizhou–Sichuan border region, and joins the Yangtze River in Hejiang County, Sichuan Province. The basin has an overall elevation difference of approximately 1580 m and exhibits a broad geomorphic transition from relatively steep mountain-gorge settings in the upper basin to hilly valley landscapes downstream. This topographic gradient provides a suitable spatial setting for examining spatial variability in gravel grain-size characteristics across different parts of the basin.

A distinctive characteristic of the Chishui River Basin is the coexistence of carbonate and clastic sedimentary rocks. Carbonate rocks, clastic rocks, shale, and mixed sedimentary formations are distributed across different parts of the basin, producing a heterogeneous geological setting in which karst and non-karst terrains are spatially interspersed. The basin can therefore be regarded as a representative karst–clastic rock composite watershed in Southwest China. This geological configuration is particularly relevant to gravel deposits in riparian zones because carbonate and clastic lithologies differ in weathering processes, insoluble material production, runoff pathways, and sediment-delivery characteristics. Their coexistence within the same drainage network provides a natural setting for examining how heterogeneous geological backgrounds are reflected in gravel grain-size structure within riparian zones.

The basin is underlain mainly by carbonate rocks, clastic rocks, and shale, resulting in substantial lithological heterogeneity. Weathering and disintegration of these lithologies can generate sediment with contrasting grain-size characteristics, and lithological variation is therefore considered a potential background factor contributing to spatial differences in riparian gravel characteristics. The basin has a subtropical monsoon climate, with annual precipitation of approximately 1000–1300 mm, most of which occurs between May and September. Seasonal rainfall and flood events provide an important hydrological setting for hillslope erosion, sediment delivery, and bed-material reworking. However, because long-term sediment supply was not directly measured in this study, these processes are

treated as potential environmental influences rather than directly demonstrated controls on the observed grain-size patterns.

For basin-scale comparison of gravel grain-size characteristics, sampling sites were grouped into three broad longitudinal zones according to elevation: an upstream zone (379–700 m), a midstream zone (248–378 m), and a downstream zone (171–247 m) (Figure 1). For sites located on tributaries, the elevation of the tributary confluence with the Chishui mainstem was used as the reference for longitudinal grouping. The boundaries between the three zones were referenced to the mainstem sections near Maotai and Chishui City, which are commonly used as longitudinal division points in studies of the Chishui River. The corresponding elevation thresholds of approximately 379 m and 248 m were determined with reference to these mainstem locations and the elevation distribution of the sampling sites, providing a consistent spatial framework for basin-scale comparisons. Importantly, these zones represent broad basin-scale elevation–longitudinal groups rather than a continuous sequence of sites along a single mainstem channel. Accordingly, the terms upstream, midstream, and downstream are used to compare gravel grain-size characteristics among broad parts of the basin, rather than to represent a continuous downstream sequence of the 15 sampling sites.

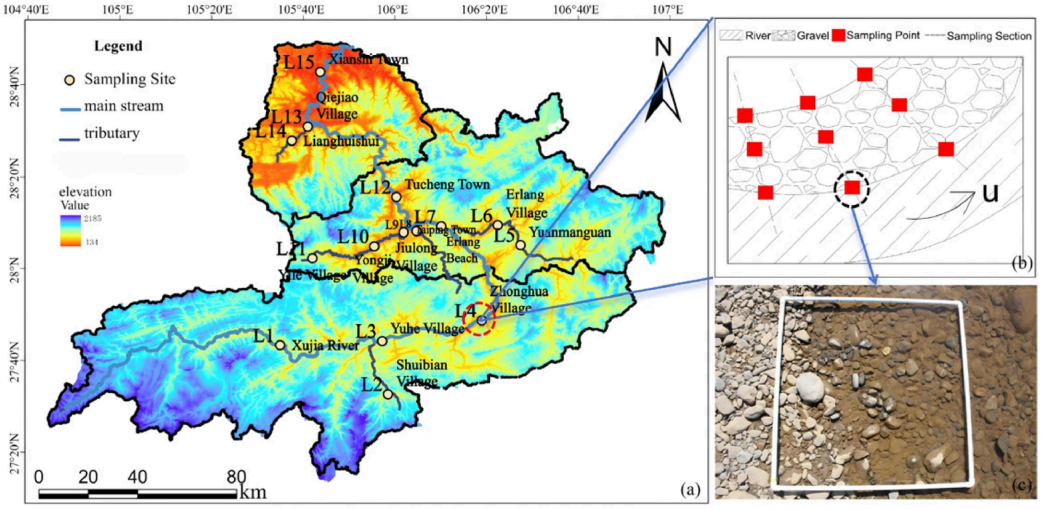


Figure 1. Location of the study area and sampling strategy in the Chishui River Basin. (**a**) location of the Chishui River Basin and distribution of sampling sites; (**b**) schematic diagram of the sampling section; (**c**) field photograph of the quadrat used for gravel sampling.

2.2. Sampling Design

To characterize spatial variability in gravel grain-size properties across the Chishui River Basin, approximately 25 field-survey locations were initially distributed throughout the basin to provide broad coverage of different river reaches and geomorphic settings. During field investigation, some locations lacked suitable exposed gravel deposits for grain-size analysis, while images obtained at several other locations were unsuitable for subsequent particle delineation and grain-size extraction because of obstruction, field conditions, or insufficient image quality. After screening for gravel visibility and image usability, 15 valid sampling sites were retained for subsequent analysis. Of these 15 sites, four were located in the upstream zone (L1–L4), eight in the midstream zone (L5–L12), and three in the downstream zone (L13–L15). Each sampling site was treated as an independent statistical unit in subsequent regional comparisons. These retained sites included locations on the mainstem and tributaries, and their assignment to the upstream, midstream, and downstream groups followed the criteria described in Section 2.1.

At each surveyed location, sampling positions were established according to the degree of bar exposure and local topographic conditions. In principle, up to three cross-sections were arranged longitudinally within each surveyed reach, and representative positions were selected along transects perpendicular to the flow direction, including locations near the active water edge, in the central part of the exposed bar, and farther from the water near the bank side. A 1 m × 1 m quadrat was established at each accessible sampling position. Because bar exposure, local topography, gravel distribution, and field accessibility varied among sites, valid images could not be obtained from every planned sampling position. Consequently, the number of usable photographs differed among sites, with a maximum of nine quadrat images available for an individual site.

For subsequent analysis, gravel particles were identified and measured separately from each valid image. All valid particles extracted from the images belonging to the same sampling site were pooled to construct a single site-level grain-size dataset, from which conventional grain-size descriptors and multifractal parameters were calculated. Accordingly, the sampling site, rather than the individual photograph or quadrat, was treated as the statistical unit in subsequent analyses. Multiple quadrats were used primarily to increase spatial coverage of surface gravel within each site and were not treated as independent replicates in among-site statistical comparisons.

2.3. Image Acquisition, Processing, and Gravel Grain-Size Extraction

Image-based and photogrammetric approaches have been increasingly applied to characterize riverbed morphology and sediment properties in fluvial environments [13–15]. Digital images of each 1 m × 1 m quadrat were acquired using a Nikon Z5 camera with an original image resolution of 6016 × 4016 pixels. During image acquisition, the camera was positioned approximately 1 m above the gravel surface, and the optical axis was kept as close as possible to perpendicular to the gravel surface in order to minimize perspective distortion. Because perfectly vertical photography could not always be maintained under field conditions owing to local topography and practical constraints, some images still exhibited a degree of perspective distortion. All images used for subsequent analysis were therefore cropped and geometrically rectified in Adobe Photoshop CC2019 using the 1 m × 1 m quadrat frame as a geometric reference, with the aim of restoring the quadrat as closely as possible to a regular square.

After geometric correction, the images were imported into ImageJ 1.54 for gravel-particle delineation and grain-size measurement [16–19]. Because particle contact, local shadows, and color variability on natural gravel surfaces may reduce the reliability of fully automated segmentation, gravel particles were manually delineated in ImageJ according to their visible boundaries in the original images. All particle delineation and identification were performed by a single operator. Uniform delineation criteria were applied to all images to ensure consistency in particle identification and measurement. Only particles with clearly distinguishable boundaries were included, and partially occluded particles were excluded when more than 50% of their estimated projected area was obscured. For adjacent or overlapping particles, individual particles were retained only when their visible boundaries could be reliably distinguished. Particles intersecting the quadrat boundary were excluded when more than 20% of their estimated perimeter was visually judged to be truncated by the sampling frame. The geometric parameters of the retained particles were subsequently extracted using ImageJ [15,18,20]. The workflow of image processing and gravel grain-size extraction is illustrated in Figure 2.

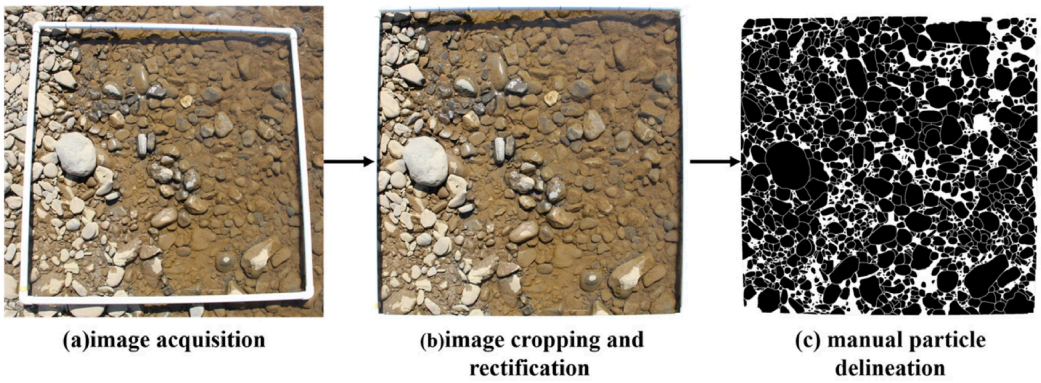


Figure 2. Workflow of gravel grain-size extraction from quadrat images. (**a**) image acquisition; (**b**) image cropping and rectification; (**c**) manual particle delineation.

Image scale was calibrated using the 1 m × 1 m quadrat visible in each photograph. In representative rectified images, a 1 m side of the quadrat corresponded to approximately 2067 pixels, equivalent to a spatial resolution of approximately 0.48 mm pixel^{-1}. Because acquisition angle and the degree of perspective correction differed slightly among photographs, the quadrat in each image was used as the scale reference for converting pixel measurements to physical lengths rather than assuming an identical pixel-to-length conversion for all images.

For each manually delineated gravel particle, the maximum Feret diameter F_{max} and minimum Feret diameter F_{min} were extracted in ImageJ [21,22]. To provide a representative measure incorporating both the long- and short-axis dimensions of the particle in the two-dimensional image, particle size d_F was calculated as the Euclidean norm of the two Feret diameters:

$$d_F = \sqrt{F_{\max}^2 + F_{\min}^2}, \quad (1)$$

where F_{max} and F_{min} represent the maximum and minimum Feret diameters of the particle measured from the two-dimensional image, respectively. Particle-size measurements obtained from all valid images within the same sampling site were pooled, as described in Section 2.2, to construct a single site-level grain-size dataset.

From the pooled particle-size dataset for each site, mean grain size, standard deviation, coefficient of variation (CV), median grain size (D_{50}), and the proportions of different grain-size classes were calculated. Particles smaller than 10 cm were classified as fine gravel, those between 10 and 20 cm as medium gravel, and those larger than 20 cm as coarse gravel. The proportion of each grain-size class was calculated as the percentage of particles falling within the corresponding size interval relative to the total number of valid particles identified at that site.

Because grain-size measurements were derived from two-dimensional images of exposed gravel surfaces, the resulting dataset primarily represents particles satisfying the established identification and delineation criteria. Although these criteria reduced potential errors associated with particle occlusion and indistinct boundaries, measurement uncertainty may remain for particles approaching the spatial resolution of the images. The smallest recorded particle size was approximately 0.71 mm, compared with a representative image resolution of 0.48 mm pixel^{-1}. To assess the influence of these smallest particles on conventional grain-size statistics, sensitivity analyses were conducted by excluding particles smaller than 2 and 3 mm. Only 9 particles (0.088% of the total) were smaller than 2 mm, while 19 particles (0.185%) were smaller than 3 mm. After excluding particles smaller than 3 mm, changes in site-level mean grain size and D_{50} were less than 1%, indicating limited sensitivity of these conventional descriptors to the smallest measured particles. Neverthe-

less, the minimum recorded particle size represents the lower bound of the extracted dataset rather than an independently validated minimum reliably measurable size.

2.4. Multifractal Analysis Approach

To further characterize the structure of gravel grain-size distributions across different scales and probability levels, multifractal analysis was applied to the pooled site-level grain-size datasets. The identified gravel particles ranged from 0.07 to 141.07 cm. This grain-size range was first logarithmically transformed and divided into 100 elementary intervals of equal logarithmic width. For each sampling site, the number of particles within each interval was counted, and the proportion of particles within that interval relative to the total number of valid particles at the site was used as its probability.

A box-counting framework was then applied to the logarithmically transformed grain-size range. The full range was successively divided into 2, 4, 8, 16, 32, and 64 subintervals, corresponding to scales ε of 2, 1, 0.5, 0.25, 0.125, and 0.0625, respectively. At a given scale ε, the probability within the *jth* subinterval was denoted by $\mu_j(\varepsilon)$ and calculated as the sum of the probabilities of the elementary grain-size intervals contained within that subinterval. Changes in the probability structure of the grain-size distribution could therefore be evaluated across different partition scales. For a statistical moment order q, the partition function was defined as

$$Z(q,\varepsilon) = \sum_{j=1}^{N(\varepsilon)} \left[\mu_j(\varepsilon)\right]^q, \tag{2}$$

The partition function was evaluated only over occupied grain-size intervals with positive probability masses ($\mu j(\varepsilon) > 0$). Empty intervals were excluded from the summation because negative powers of zero are mathematically undefined, and no artificial probability values were assigned to these intervals. The moment order q ranged from −10 to 10, with an increment of 1, to characterize grain-size subsets across a broad range of occurrence probabilities. Negative moment orders emphasize low-probability grain-size intervals, whereas positive moment orders assign greater weight to dominant grain-size fractions. This symmetric range was selected to characterize the contrasting scaling behavior of low- and high-probability subsets. Given the sensitivity of large negative moment orders to sparsely occupied intervals, the resulting estimates were interpreted with consideration of this numerical limitation.

For $q \neq 1$, the generalized dimension D_q was calculated as:

$$D_q = \lim_{\varepsilon \to 0} \frac{1}{q-1} \frac{\lg\left(\sum_{j=1}^{N(\varepsilon)} \mu_j(\varepsilon)^q\right)}{\lg\varepsilon} (q \neq 1), \tag{3}$$

For q = 1, the information dimension D1 was calculated as:

$$D_1 = \lim_{\varepsilon \to 0} \frac{\sum_{j=1}^{N(\varepsilon)} \mu_j(\varepsilon) \lg \mu_j(\varepsilon)}{\lg\varepsilon} (q = 1), \tag{4}$$

In practice, D_q was estimated using least-squares linear regression of the corresponding logarithmic scaling relationships across the selected scales. A systematic variation in D_q with q indicates a non-uniform scaling structure, whereas a greater variation in D_q across the q-range reflects a stronger contrast among grain-size subsets with different occurrence probabilities.

The information dimension (D_1) and correlation dimension (D_2) were used to characterize the probability-weighted scaling structure of grain-size distributions. D_1 reflects the

information distribution across grain-size intervals, whereas D_2 assigns greater weight to intervals with higher probability masses. Unlike these probability-weighted dimensions, the capacity dimension (D_0) depends solely on the number of occupied intervals, irrespective of their probability masses. During methodological reassessment, the original finite-scale estimates of D_0 were found to exceed the theoretical upper bound of unity for a one-dimensional grain-size distribution. This discrepancy may be associated with sensitivity to partition boundaries and uncertainty in finite-scale estimation. Although D_0 and the other generalized dimensions are derived from the same grain-size probability distribution and partition scales, different moment orders involve distinct probability-weighting mechanisms, and the estimation of Dq at $q \neq 0$ does not directly depend on the estimated value of D_0. Therefore, anomalous D_0 estimates do not necessarily imply errors of the same magnitude in the remaining generalized dimensions. Accordingly, the remaining generalized dimensions and associated spectral descriptors were retained for characterizing relative variations in grain-size probability distributions, with due consideration of finite-scale uncertainty and the sensitivity of negative moment orders. The original D_0 estimates were retained solely as an exploratory visual reference for the variation trends of the generalized-dimension spectrum rather than as quantitative descriptors.

The width of the generalized-dimension spectrum was calculated as $\Delta D = D_{-10} - D_{10}$. A larger ΔD indicates a greater difference between the generalized dimensions associated with low- and high-probability grain-size subsets and therefore stronger structural heterogeneity across probability levels. In this study, ΔD was treated as a descriptor of cross-probability scaling heterogeneity. Its structural significance was subsequently evaluated in relation to conventional grain-size descriptors rather than being assigned to a specific sedimentary process a priori.

Local multifractal characteristics were further described using the singularity exponent $\alpha(q)$ and the multifractal spectrum $f[\alpha(q)]$. For a given q and scale ε, the normalized probability weight was defined as:

$$\mu_j(q,\varepsilon) = \frac{\left[\mu_j(\varepsilon)\right]^q}{\sum_{j=1}^{N(\varepsilon)}\left[\mu_j(\varepsilon)\right]^q}, \tag{5}$$

The singularity exponent was calculated as:

$$\alpha(q) = \lim_{\varepsilon\to 0}\frac{\sum_{j=1}^{N(\varepsilon)}\mu_j(q,\varepsilon)\lg\mu_j(\varepsilon)}{\lg\varepsilon}, \tag{6}$$

and the corresponding multifractal spectrum as:

$$f(\alpha(q)) = \lim_{\varepsilon\to 0}\frac{\sum_{j=1}^{N(\varepsilon)}\mu_j(q,\varepsilon)\lg\mu_j(q,\varepsilon)}{\lg\varepsilon}, \tag{7}$$

The relationship between $\alpha(q)$ and $f[\alpha(q)]$ was used to characterize local scaling properties and structural complexity associated with grain-size subsets of different probabilities.

The width of the singularity spectrum was calculated as $\Delta\alpha = \alpha_{max} - \alpha_{min}$. A larger $\Delta\alpha$ indicates a broader range of local scaling behavior among different probability subsets.

Spectrum asymmetry was characterized using $\Delta f = f(\alpha_{min}) - f(\alpha_{max})$, where $f(\alpha_{min})$ and $f(\alpha_{max})$ represent the multifractal spectrum values at the minimum and maximum singularity exponents, respectively. A negative Δf indicates that $f(\alpha_{min})$ is smaller than $f(\alpha_{max})$, reflecting an asymmetry in the relative spectral dimensions associated with the two ends of the singularity spectrum. Under the reference moment-order range ($q = -10$

to 10) adopted in this study, the negative Δf values indicate a similar direction of spectral asymmetry across the sampled sites. Unlike ΔD and $\Delta\alpha$, which describe the widths of the generalized-dimension and singularity-exponent ranges, respectively, Δf characterizes the difference between the spectral values at the two endpoints. Accordingly, the sign of Δf was interpreted as a mathematical characteristic of the singularity spectrum rather than direct evidence of a specific sediment-transport or depositional process.

To assess the sensitivity of the multifractal descriptors to the selected moment-order range, additional calculations were conducted using q ranges of −2 to 2, −3 to 3, −5 to 5, and −7 to 7, with −10 to 10 as the reference. The relative rankings of sampling sites remained highly consistent across the tested ranges, with Spearman rank correlation coefficients of 0.979–0.989 for ΔD, 0.975–0.993 for $\Delta\alpha$, and 0.929–0.986 for Δf. However, the absolute magnitudes and, in some cases, the signs of these descriptors varied with the moment-order limits. These results indicate that relative site-to-site patterns were less sensitive to the selected q range than the absolute spectral estimates.

Overall, D_1, D_2, ΔD, $\Delta\alpha$, and Δf were used to characterize the multifractal properties of gravel grain-size distributions at individual sampling sites.

2.5. Statistical Analysis

All statistical analyses were conducted at the sampling-site level using the 15 retained sites. Sites were grouped into upstream, midstream, and downstream zones as described in Section 2.1.

Flow velocity and water depth were measured in situ at one representative location within the cross-section of each monitoring site using a portable current meter (LGY-II) and a depth rod, respectively. Under relatively stable flow conditions, three consecutive velocity readings were obtained at the same location, and their arithmetic mean was used as the site-level velocity observation. These repeated measurements were intended to reduce short-term measurement variability. The recorded values were considered indicative of local hydraulic conditions during the corresponding sampling campaign rather than cross-sectionally averaged or seasonally representative hydraulic conditions.

Differences in conventional grain-size descriptors and multifractal parameters among the three zones were evaluated using one-way analysis of variance (ANOVA). The normality of ANOVA residuals and homogeneity of variances were assessed using the Shapiro–Wilk and median-centered Levene tests, respectively. Effect sizes were quantified using eta-squared (η^2), calculated as the ratio of between-group sum of squares to total sum of squares. To assess the uncertainty of regional differences, 95% confidence intervals for pairwise mean differences were estimated using Welch's method. Given the limited and unequal group sample sizes and departures from normality for some variables, Kruskal–Wallis tests were additionally performed as a nonparametric sensitivity analysis. A significance level of $p < 0.05$ was adopted for group comparisons.

Spearman rank correlation analysis was conducted at the sampling-site level ($n = 15$) to evaluate associations between conventional grain-size descriptors and multifractal parameters [23]. The original cross-category analysis included seven conventional descriptors (fine-, medium-, and coarse-gravel proportions, mean grain size, standard deviation, coefficient of variation, and D_{50}) and three multifractal descriptors (ΔD, $\Delta\alpha$, and Δf). To control the false discovery rate, the Benjamini–Hochberg (BH) procedure was applied to all 21 original cross-category correlations [24]. All tests were two-tailed, and a BH-adjusted q-value below 0.05 was considered statistically significant. To reduce redundancy in the presentation, six selected correlations involving D_{50}, CV, SD, ΔD, and Δf are reported below. Statistical analyses were performed using IBM SPSS Statistics 19.0 (IBM Corp., Armonk, NY, USA).

In addition, exploratory Spearman correlations were used to examine whether the observed site-to-site grain-size variability was associated with available site-level channel slope and flow-velocity measurements. This analysis included the 10 sites with unambiguous environmental records, with the midpoint of the recorded slope range used as the representative site-level slope.

3. Results

3.1. Spatial Variability in Conventional Gravel Grain-Size Characteristics

Surface gravel in riparian zones at the 15 sampling sites in the Chishui River Basin exhibited pronounced variability among individual sites, with identified particle sizes ranging from 0.07 to 141.07 cm. Grain-size composition, mean grain size, and dispersion varied substantially among sampling locations (Table 1).

Table 1. Conventional grain-size characteristics at sampling sites across the Chishui River Basin.

Reach	Site	Fine Gravel (%) (<10 cm)	Coarse Gravel (%) (>20 cm)	Mean Size (cm)	Standard Deviation (cm)	*CV*	Size Range (cm)	D_{50} (cm)	Slope (°)	Velocity ($m \cdot s^{-1}$)
Upstream	L1	88.12	3.03	4.743	5.625	1.186	0.095–45.868	2.643	8–18	0.4175
	L2	87.07	1.06	5.665	4.154	0.733	0.649–34.066	4.571	2–10	0.4097
	L3	42.75	36.23	16.022	12.110	0.756	1.044–57.081	13.178	12–19	0.0686
	L4	81.19	3.68	6.621	5.626	0.850	0.384–35.465	4.866	3–10	0.0477
	Mean	74.78	11.00	8.26	6.88	0.881	0.095–57.081	6.31	6.2	0.2359
Midstream	L5	54.66	23.60	13.520	12.430	0.919	1.122–70.611	8.862	No data	No data
	L6	58.86	18.29	11.718	10.160	0.867	1.007–52.670	7.673	No data	No data
	L7	94.78	0.97	3.911	4.008	1.025	0.071–84.445	2.882	5–13	0.1444
	L8	76.11	8.89	8.694	8.137	0.936	1.159–64.655	6.099	No data	No data
	L9	84.44	6.38	6.958	10.112	1.453	0.973–85.267	3.621	2–18	1.75
	L10	91.85	1.08	4.863	3.979	0.818	0.121–33.925	3.631	2–14	0.2982
	L11	70.13	8.66	8.924	9.495	1.064	1.000–83.092	5.881	No data	No data
	L12	74.26	5.06	8.296	6.615	0.797	1.128–55.386	6.504	8–22	0.1315
	Mean	75.64	9.12	8.36	8.12	0.985	0.071–85.267	5.64	9.1	0.2130
Downstream	L13	75.93	9.54	8.964	11.598	1.294	0.640–85.712	5.309	14–15	0.1187
	L14	49.84	30.62	17.735	18.989	1.071	1.082–141.071	10.008	8–30	0.4472
	L15	91.43	1.4	5.406	3.626	0.671	0.881–23.157	4.130	9–19	0.2846
	Mean	72.40	13.86	10.70	11.40	1.012	0.640–141.071	6.48	13.7	0.2835

Fine gravel dominated at most sampling sites, although its proportion varied considerably among locations. Fine-gravel content ranged from 42.8% to 94.8%, medium-gravel content from 4.2% to 22.9%, and coarse-gravel content from 1.0% to 36.2%. L7 had the highest proportion of fine gravel (94.8%), whereas L3 had the lowest (42.8%). Coarse gravel was particularly abundant at L3 and L14, accounting for 36.2% and 30.6% of the identified particles, respectively. Overall, grain-size composition varied markedly among individual sampling sites.

At the regional scale, mean grain-size composition was broadly similar among the upstream, midstream, and downstream groups. Mean proportions of fine, medium, and coarse gravel were 74.8%, 14.2%, and 11.0% in the upstream group; 75.6%, 15.2%, and 9.1% in the midstream group; and 72.4%, 13.7%, and 13.9% in the downstream group, respectively. Neither fine-gravel enrichment nor coarse-gravel depletion showed a monotonic downstream pattern, and the proportions of fine, medium, and coarse gravel did not differ significantly among the three groups (all $p > 0.05$).

Mean grain size ranged from 3.91 to 17.74 cm among sites, whereas D_{50} ranged from 2.64 to 13.18 cm. Mean grain size was 8.26, 8.36, and 10.70 cm in the upstream, midstream, and downstream groups, respectively, while mean D_{50} values were 6.31, 5.64, and 6.48 cm. Neither mean grain size nor D_{50} differed significantly among the three groups ($p > 0.05$). L14 had the largest mean grain size (17.74 cm), whereas L7 had the smallest (3.91 cm), indicating marked variability among individual sampling sites.

Grain-size dispersion also varied considerably among sites. Standard deviation ranged from 3.63 to 18.99 cm and *CV* from 0.67 to 1.45. Mean *CV* values were 0.88, 0.99, and 1.01 in the upstream, midstream, and downstream groups, respectively. No clear monotonic increase or decrease in *CV* was observed along the upstream-to-downstream sequence, and differences among the three groups were not significant ($p > 0.05$).

Overall, conventional grain-size statistics revealed pronounced variability among individual sampling sites; however, this variability did not translate into a clear monotonic upstream-to-downstream pattern, and none of the major conventional grain-size descriptors differed significantly among the three longitudinal groups.

3.2. Cumulative Grain-Size Distribution Characteristics

Cumulative frequency curves of gravel grain size differed markedly among sampling sites in their position, slope, and the extent of coarse-grained tails (Figure 3).

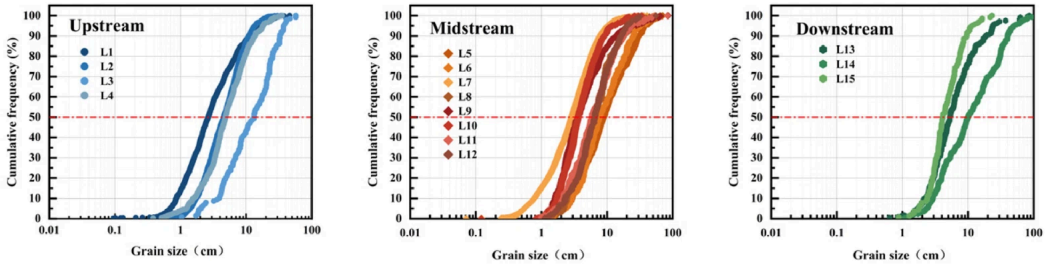


Figure 3. Cumulative frequency distributions of gravel grain size in riparian zones at the 15 sampling sites in the Chishui River Basin. Curves were calculated from all identified gravel particles pooled within each sampling site.

Clear differences were evident among the upstream sites. The cumulative curves for L1, L2, and L4 were generally shifted toward smaller grain sizes, with D_{50} values of 2.64, 4.57, and 4.87 cm, respectively. In contrast, the curve for L3 was distinctly shifted toward coarser grain sizes, with a D_{50} of 13.18 cm and a more pronounced coarse-grained tail. These patterns indicate that grain-size distribution shapes were not uniform among the upstream sites.

Substantial within-group variability was also observed among the midstream sites. The curves for L7 and L10 were concentrated toward smaller grain sizes, with corresponding D_{50} values of 2.88 and 3.63 cm. In contrast, the curves for L5 and L6 were shifted toward coarser sizes, with D_{50} values of 8.86 and 7.67 cm, respectively. The remaining midstream sites occupied intermediate positions, showing different degrees of grain-size concentration and extension of coarse-grained tails.

The three downstream sites likewise exhibited contrasting cumulative distributions. The curve for L15 was shifted toward smaller grain sizes, with a D_{50} of 4.13 cm, whereas L13 had a D_{50} of 5.31 cm. In contrast, the curve for L14 was distinctly shifted toward coarser grain sizes, with a D_{50} of 10.01 cm and a more extended coarse-grained tail. L14 also contained the largest particle recorded in the study, with a grain size of 141.07 cm.

Overall, the cumulative frequency curves showed clear differences among sites in curve position, slope, and the extent of coarse-grained tails. Within the same longitudinal

zone, sites with relatively concentrated grain-size distributions coexisted with sites characterized by broader distributions and more pronounced coarse-grained tails, highlighting the complexity of gravel grain-size distributions among sampling sites.

3.3. Multifractal Characteristics of Grain-Size Organization Across Scales

3.3.1. Generalized Dimension Spectrum Characteristics

The $D_q - q$ curves of all 15 sampling sites decreased monotonically with increasing q and exhibited distinct inverse-S-shaped nonlinear forms (Figure 4). The magnitude of change differed between the negative- and positive-q ranges, indicating different scaling responses of low- and high-probability grain-size components. The generalized-dimension spectra showed broadly similar variation patterns across sampling sites, although differences in curve shape and magnitude were observed.

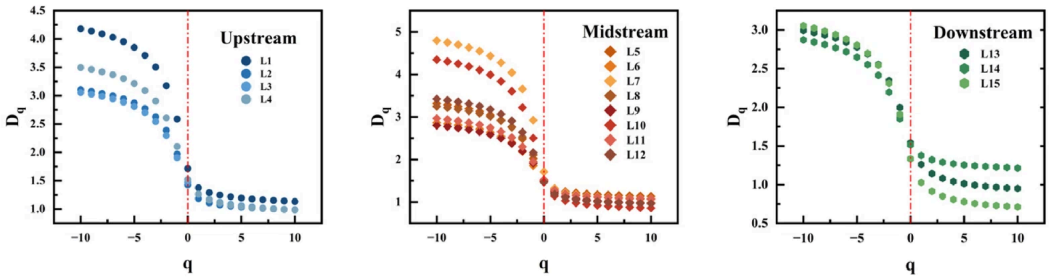


Figure 4. Generalized dimension spectrum curves D_q-q for the gravel samples. The D_0 estimates are presented solely as an exploratory visual reference for the variation trends of the generalized-dimension spectrum and are not interpreted as valid quantitative estimates of the capacity dimension.

Generalized-dimension parameters varied among individual sampling sites. Values of D_1, and D_2 ranged from 1.03 to 1.38, and 0.91 to 1.32, respectively. Mean values of these two parameters were 1.27, and 1.18 in the upstream group; 1.25, and 1.16 in the midstream group; and 1.22, and 1.13 in the downstream group. Overall, the regional means of the three parameters showed a slight decrease from upstream to downstream, although the differences among groups were not statistically significant.

In contrast, the spectral width ΔD showed more pronounced site-to-site variability, ranging from 1.66 to 3.72. Mean ΔD values were 2.44, 2.46, and 2.01 in the upstream, midstream, and downstream groups, respectively. Although the downstream mean was relatively lower, differences among the three groups were not statistically significant. At the site level, L7 and L10 had relatively high ΔD values of 3.72 and 3.49, respectively, whereas the lowest value occurred at L14, indicating substantial variation among sites in the scaling contrast between high- and low-probability grain-size components.

Overall, the generalized-dimension spectra exhibited nonlinear variations across moment orders, with differences in parameter variability among sampling sites. The regional means of D_1 and D_2 showed relatively limited variation, whereas ΔD exhibited more pronounced site-level fluctuations. These results indicate that the scaling characteristics of gravel grain-size distributions varied among individual sampling sites without forming a statistically significant upstream–midstream–downstream differentiation.

3.3.2. Singularity Spectrum Characteristics

The $f(\alpha) - \alpha$ curves of all 15 sampling sites exhibited continuous, asymmetric unimodal forms (Figures 5 and 6), further supporting the presence of the multifractal characteristics of gravel grain-size distributions in riparian zones. The singularity spectra varied among

sites in both spectral width and asymmetry, with $\Delta\alpha$ describing differences in local scaling characteristics among grain-size components with different probabilities.

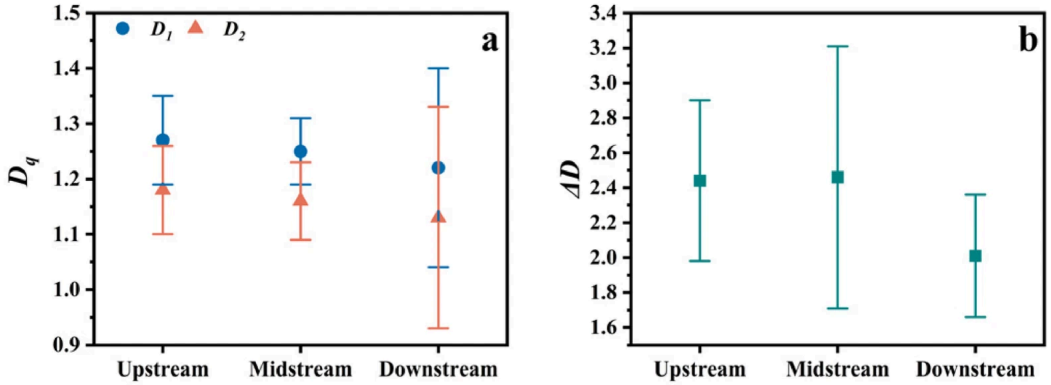


Figure 5. Regional comparison of multifractal parameters of gravel grain-size distributions. (**a**) Generalized dimensions D_1, and D_2; (**b**) ΔD. Values are presented as mean ± SD for the upstream, midstream, and downstream zones. No significant differences were detected among the three longitudinal zones for any parameter (one-way ANOVA, $p > 0.05$).

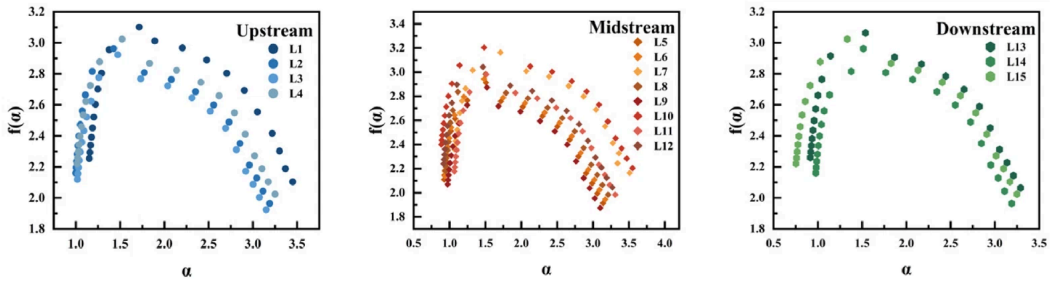


Figure 6. Multifractal singularity spectrum curves $f(\alpha)$-α for the gravel samples.

Values of $\Delta\alpha$ ranged from 2.13 to 2.66 among the sampling sites. Mean values were 2.21, 2.32, and 2.36 in the upstream, midstream, and downstream groups, respectively. Although the regional means increased slightly downstream, the differences among the three groups were not statistically significant. At the site level, L10 had the largest $\Delta\alpha$ value, followed by L15, whereas L9 had the smallest value, indicating appreciable variation in singularity-spectrum width among individual sites.

Compared with $\Delta\alpha$, Δf showed substantially less variation(Figure 7). Under the reference moment-order range ($q = -10$ to 10), Δf values were negative at all 15 sites, ranging from −0.197 to −0.150. Except for L1, the remaining sites were concentrated within a narrow range from −0.192 to −0.197. Mean Δf values were approximately −0.185, −0.196, and −0.196 in the upstream, midstream, and downstream groups, respectively, and were broadly similar among the three zones. Under the adopted moment-order range, the negative Δf values indicate a common direction of singularity-spectrum asymmetry across the sampling sites, while their narrow range indicates relatively limited variation in the degree of spectral asymmetry among most sites.

Overall, $\Delta\alpha$ and Δf exhibited contrasting patterns of variability. Whereas $\Delta\alpha$ varied appreciably among individual sampling sites, Δf remained relatively stable and negative across all sites under the adopted moment-order range. This contrast suggests that spectral width and spectral asymmetry may reflect different aspects of the observed multifractal structure, consistent with their distinct mathematical definitions.

Regional comparisons of the five retained multifractal descriptors (D_1, D_2, ΔD, $\Delta\alpha$, and Δf) revealed no statistically significant differences among the three basin zones according to

either ANOVA or Kruskal–Wallis tests (all $p > 0.05$). The estimated effect sizes (η^2) ranged from 0.039 to 0.181 across the five descriptors.

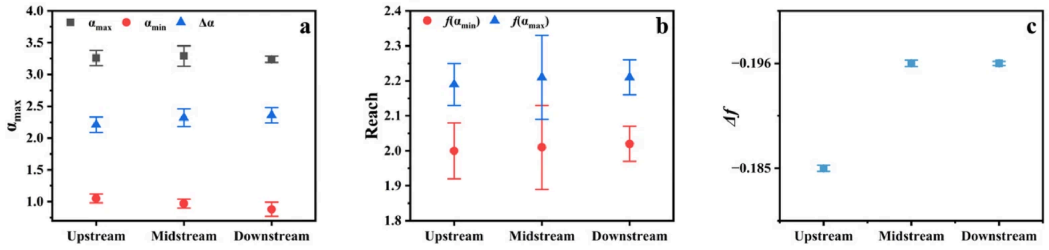


Figure 7. Regional comparison of singularity-spectrum parameters of gravel grain-size distributions. (**a**) α_{max}, α_{min}, and $\Delta\alpha$; (**b**) $f(\alpha_{min})$ and $f(\alpha_{max})$; and (**c**) Δf. The Δf values correspond to the reference moment-order range of $q = -10$ to 10. Values are presented as mean ± SD for the upstream, midstream, and downstream zones. No significant differences were detected among the three longitudinal zones for any parameter (one-way ANOVA, $p > 0.05$).

3.3.3. Consistency and Divergence Between Multifractal and Conventional Grain-Size Descriptors

Spearman correlation analysis was conducted to examine the relationships between conventional grain-size descriptors and multifractal parameters (Table 2). Considering the correlations among the original indicators, D_{50}, CV, and SD were selected to represent median grain size, relative dispersion, and absolute dispersion, respectively, while ΔD and Δf were retained to characterize different aspects of the multifractal spectrum. To account for multiple comparisons, the Benjamini–Hochberg (BH) procedure was applied to all 21 original cross-category correlations.

Among the six reported correlations, SD exhibited a significant negative correlation with ΔD ($\rho = -0.750$, BH-adjusted $q = 0.013$), indicating that sampling sites with greater absolute grain-size dispersion tended to exhibit smaller ΔD values. D_{50} was negatively associated with ΔD ($\rho = -0.561$), whereas CV was positively associated with Δf ($\rho = 0.563$); however, neither relationship remained statistically significant after BH correction (both $q = 0.067$). The remaining correlations were also nonsignificant ($q > 0.05$). Thus, SD–ΔD was the only statistically significant association among the selected indicator pairs after correction.

Table 2. Spearman correlations between selected conventional grain-size descriptors and multifractal parameters.

Grain-Size Descriptor	ΔD	Δf
D_{50}	−0.561	−0.145
CV	−0.296	0.563
SD	−0.750 *	0.245

Note: Values represent Spearman's rank correlation coefficients (ρ). * indicates statistical significance after Benjamini–Hochberg (BH) correction across the original 21 comparisons (adjusted q < 0.05).

4. Discussion

4.1. Descriptive Contribution of Multifractal Analysis to Gravel Grain-Size Characterization

Conventional grain-size descriptors and multifractal parameters characterize different statistical properties of gravel grain-size distributions. Conventional descriptors primarily summarize particle-size magnitude, composition, and dispersion, whereas multifractal analysis examines the probability-dependent scaling behavior of grain-size distributions across different moment orders and partition scales [6,10,12]. Specifically, the generalized-

dimension spectrum width (ΔD) quantifies the variation in generalized dimensions across the selected moment orders, the singularity-spectrum width ($\Delta\alpha$) describes the range of singularity exponents, and the singularity-spectrum asymmetry (Δf) characterizes the difference between the spectral values at the two endpoints. These parameters describe variations in the probability structure and spectral characteristics of grain-size distributions, providing a quantitative basis for examining distributional properties beyond conventional measures of particle-size magnitude and dispersion.

Spearman correlation analysis identified a significant negative association between standard deviation (SD) and ΔD ($\rho = -0.750$, BH-adjusted $q = 0.013$). Across the 15 sampling sites, greater absolute grain-size dispersion tended to coincide with a narrower generalized-dimension spectrum. *SD* quantifies the absolute spread of particle sizes, whereas ΔD describes the range of generalized dimensions associated with different probability-weighting orders. Their significant association suggests a statistical correspondence between conventional grain-size dispersion and probability-dependent scaling characteristics within the investigated dataset. This relationship provides a specific quantitative result for interpreting how variations in particle-size dispersion are associated with changes in the multifractal characteristics of riparian gravel deposits.

Other selected relationships showed different levels of statistical support. Median grain size (D_{50}) was negatively correlated with ΔD ($\rho = -0.561$), while the coefficient of variation (CV) was positively correlated with Δf ($\rho = 0.563$). However, neither relationship remained statistically significant after Benjamini–Hochberg correction (both adjusted $q = 0.067$). No significant correlations were detected between Δf and the selected conventional grain-size descriptors after correction. Furthermore, ΔD and $\Delta\alpha$ exhibited site-to-site variation, whereas Δf remained negative and relatively stable under the selected moment-order range. These differences are consistent with the distinct mathematical properties represented by the multifractal parameters: ΔD and $\Delta\alpha$ describe spectral widths, while Δf characterizes the direction and magnitude of spectral asymmetry. The observed variation therefore provides information on different features of the grain-size probability distribution without implying that the corresponding parameters are statistically independent.

Overall, the descriptive contribution of multifractal analysis in this study lies in quantifying probability-dependent scaling properties of riparian gravel grain-size distributions and establishing their observed relationships with conventional grain-size characteristics. The significant *SD*–ΔD association identifies a specific statistical connection between absolute grain-size dispersion and generalized-dimension spectrum width, while the different variation patterns of ΔD, $\Delta\alpha$, and Δf characterize distinct aspects of the observed multifractal spectra. These findings provide a quantitative basis for interpreting gravel grain-size probability distributions at the investigated sites in the Chishui River Basin. Further comparisons across additional sampling sites and geological settings may help clarify the extent to which these spectral characteristics contribute to the assessment of sediment grain-size variability.

4.2. Basin-Scale Multifractal Structure and Spatial Variability of Gravel Grain Size in a Karst–Clastic Rock Composite Watershed

The D_{q-q} curves of all 15 sampling sites in the Chishui River Basin showed similar inverse-S shapes, indicating comparable overall trends in the scale-dependent organization of gravel grain-size probabilities across the basin. Although grain-size composition, mean grain size, and dispersion varied markedly among individual sites, the overall form of the generalized dimension spectra remained similar. This suggests that multiscale heterogeneity in grain-size distributions is not restricted to a few local sites but is a common characteristic across different parts of the Chishui River Basin. Thus, although gravel composition differs

among sampling locations, their grain-size probability distributions consistently exhibit clear multifractal properties.

At the regional scale, the retained multifractal parameters showed some numerical variation among the upstream, midstream, and downstream zones, but no statistically significant longitudinal differentiation was detected. The regional mean values of D_1 and D_2 decreased slightly from upstream to downstream. Mean ΔD values were comparable between the upstream and midstream zones and somewhat lower downstream, whereas $\Delta\alpha$ showed a slight numerical increase from upstream to downstream. However, none of these regional differences was statistically significant. The multifractal parameters therefore did not form a stable gradient corresponding to the upstream–midstream–downstream classification. This pattern is consistent with the regional comparisons of conventional grain-size descriptors and suggests that longitudinal zonation provides a useful framework for broad spatial comparison but does not fully account for the observed variability in gravel grain-size structure.

Despite the absence of significant regional differentiation, several multifractal parameters exhibited pronounced site-to-site variation within the basin. In particular, ΔD and $\Delta\alpha$ varied considerably among sampling locations, reflecting differences in generalized-dimension spectrum width and singularity-spectrum width. The correlation analysis further revealed a significant negative association between SD and ΔD ($\rho = -0.750$, BH-adjusted $q = 0.013$), indicating that sites with greater absolute grain-size dispersion tended to exhibit narrower generalized-dimension spectra. By contrast, the relationships of ΔD with D_{50} and CV did not reach statistical significance after BH correction. Within the sampled sites, these findings suggest a possible correspondence between selected conventional grain-size characteristics and multifractal scaling properties.

In contrast to ΔD and $\Delta\alpha$, Δf exhibited relatively limited variation across the basin. Under the reference moment-order range ($q = -10$ to 10), its values were negative at all 15 sampling sites and, except for L1, were concentrated within a narrow range, indicating a consistent direction of singularity-spectrum asymmetry among sampling locations under the adopted calculation settings. Furthermore, Δf showed no statistically significant correlations with $D50$, CV, or SD after BH correction (all $q > 0.05$). Although the correlation between CV and Δf was moderately positive ($\rho = 0.563$), it did not remain significant after correction ($q = 0.067$). These results indicate that the relatively stable asymmetry of the singularity spectrum was not accompanied by statistically significant associations with the selected conventional grain-size descriptors, suggesting that spectral asymmetry may capture aspects of the observed distribution that are not fully reflected by the selected conventional measures.

Overall, the multifractal structure of gravel grain size in the Chishui River Basin exhibits both basin-wide consistency and substantial site-to-site variability. Sampling locations share similar generalized-dimension spectrum shapes and a consistent direction of singularity-spectrum asymmetry, whereas ΔD and $\Delta\alpha$ show more pronounced spatial variation. At the same time, no significant multifractal zonation was detected among the upstream, midstream, and downstream groups. These results indicate that longitudinal zonation alone cannot account for the observed spatial variability in gravel grain-size structure, providing a basis for further considering the possible influence of local environmental and sedimentary conditions.

4.3. Spatial Variability of Gravel Grain-Size Distributions and Possible Controls in a Karst–Clastic Rock Composite Watershed

Gravel in riparian zones of the Chishui River Basin showed pronounced site-to-site variability, but this variability did not form a continuous or monotonic upstream-to-downstream

pattern. Neither conventional grain-size descriptors nor multifractal parameters showed significant differentiation among the upstream, midstream, and downstream zones, whereas substantial differences occurred among individual sites within the same longitudinal zone. The additional statistical analyses further supported this pattern. For several conventional grain-size descriptors, the relatively small effect sizes indicated that broad basin-zone classification explained only a limited proportion of the observed site-level variability. Although some multifractal descriptors exhibited larger estimated regional effects, the Kruskal–Wallis sensitivity analysis yielded nonsignificant results consistent with those of ANOVA. These findings suggest that the observed spatial variability was not strongly differentiated by the three broad basin zones, rather than demonstrating an absence of regional differences. Moreover, the 15 sampling sites include both mainstem and tributary locations rather than representing a single continuous sediment-routing pathway. Therefore, the absence of significant regional differences should not be interpreted as an absence of spatial adjustment, but rather indicates that longitudinal position alone cannot explain the full variability observed across the basin. Local environmental and sedimentary conditions may therefore be superimposed on basin-scale sediment transfer and contribute to the observed site-to-site variability [5,25,26].

To further examine whether local environmental conditions were associated with site-to-site variability, exploratory Spearman correlations were conducted for the 10 sites with unambiguous channel-slope and flow-velocity records (Figure 8). Channel slope showed negative covariation with fine-gravel proportion ($\rho = -0.673$, $p = 0.033$) and positive covariation with coarse-gravel proportion ($\rho = 0.794$, $p = 0.006$), mean grain size ($\rho = 0.661$, $p = 0.038$), and D_{50} ($\rho = 0.648$, $p = 0.043$) at the uncorrected significance level. In contrast, slope showed no significant uncorrected relationships with CV, ΔD, or $\Delta\alpha$, and measured flow velocity was not significantly related to any of the examined conventional grain-size or retained multifractal descriptors. None of these relationships remained statistically significant after BH correction. Given the limited number of sites and incomplete environmental records, these results should be regarded as exploratory rather than evidence of deterministic environmental control. Nevertheless, the directions of the slope associations suggest that local topographic conditions may contribute to the spatial variation in gravel size observed among sites.

The tendency for coarser gravel and larger D_{50} values to occur at steeper sites is physically consistent with the general influence of channel gradient on sediment transport and local depositional conditions. However, channel slope should not be interpreted as an isolated control because the surface gravel distribution reflects the integrated effects of sediment availability, transport history, and local storage. The absence of significant relationships with measured flow velocity further illustrates this limitation. For example, L3 contained 36.23% coarse gravel and had a D_{50} of 13.18 cm despite a measured velocity of only 0.0686 m/s, whereas L14 contained 30.62% coarse gravel and had a D_{50} of 10.01 cm at a measured velocity of 0.4472 m/s. These contrasts suggest that local flow-velocity measurements obtained during individual sampling campaigns may not adequately represent the hydraulic conditions associated with the longer-term redistribution and organization of surface gravel. Riparian gravel distributions are likely to integrate sediment transport and reworking over multiple flow events, particularly during floods, rather than respond solely to the hydraulic conditions observed at the time of sampling.

Spatial differences in sediment supply and storage provide an additional context for interpreting the observed variability. Hillslope inputs, tributary contributions, bank erosion, local deposition, and subsequent reworking can modify the grain-size composition of individual reaches and interrupt simple downstream-fining patterns [27–29]. This effect may be particularly relevant in the Chishui River Basin, where carbonate rocks, clastic

rocks, shale, and mixed sedimentary formations occur within the same drainage network. Previous studies in karst watersheds of Southwest China have shown that lithology, karst configuration, basin relief, and sediment-source conditions can influence sediment production and delivery [2,3,30]. These findings provide a plausible environmental context in which spatially heterogeneous sediment supply may be superimposed on longitudinal transport. However, because lithology-specific gravel supply and sediment-source contributions were not directly quantified in the present study, geological setting cannot be identified as a demonstrated control of the observed grain-size pattern. Overall, the spatial pattern observed in the Chishui River Basin is more appropriately interpreted as the combined expression of longitudinal sediment transfer and local differences in sediment supply, transport, storage, and reworking than as a simple continuous downstream-fining sequence.

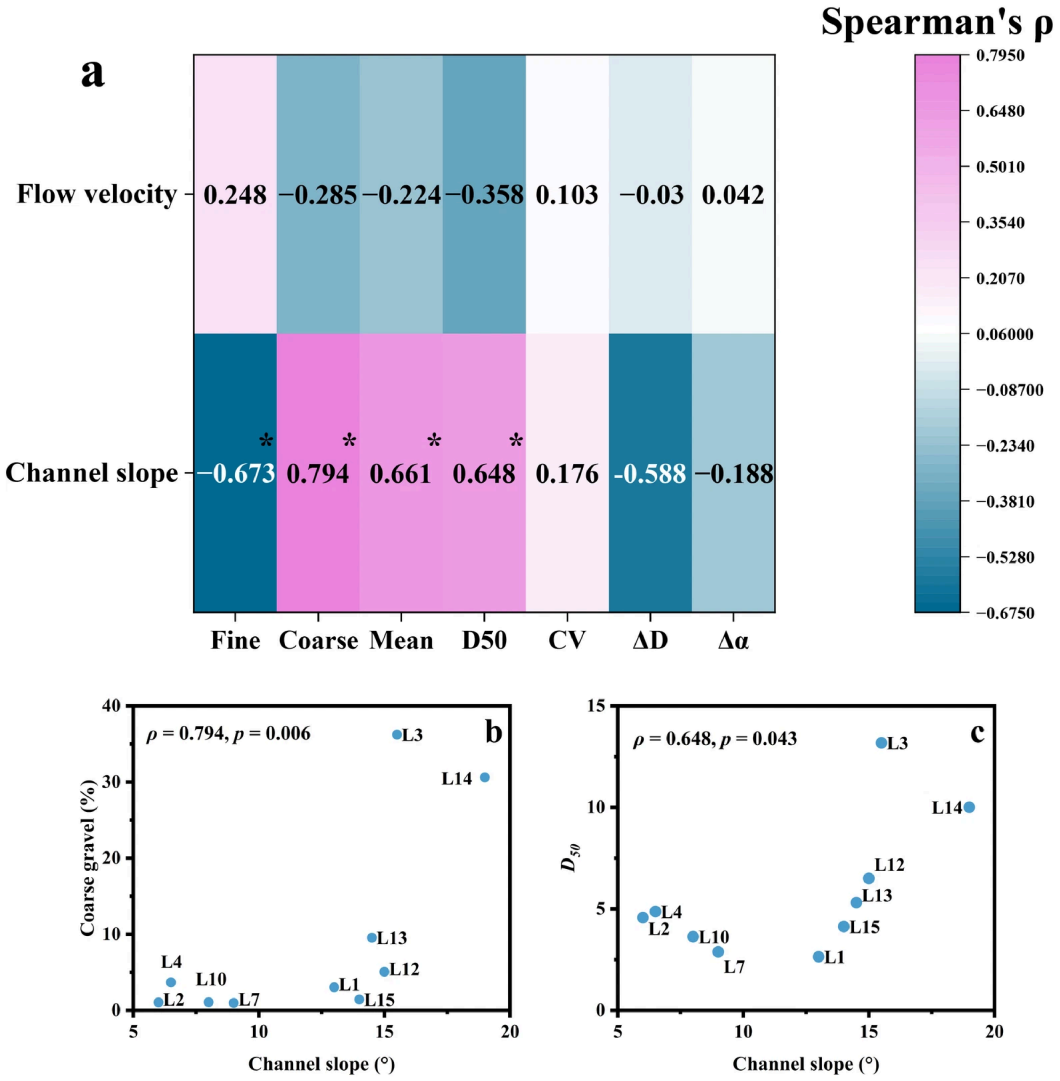


Figure 8. Exploratory relationships between available local environmental variables and gravel characteristics at sampling sites in the Chishui River Basin. (**a**) Spearman rank correlations of channel slope and measured flow velocity with selected conventional grain-size and multifractal descriptors; (**b**) relationship between channel slope and coarse-gravel proportion; and (**c**) relationship between channel slope and D_{50}. Analyses were based on the 10 sites with unambiguous environmental records, with the midpoint of the recorded slope range used as the representative site-level slope. Asterisks in (**a**) indicate uncorrected significance levels (* $p < 0.05$). None of the correlations remained statistically significant after Benjamini–Hochberg false-discovery-rate correction; therefore, these relationships are interpreted as exploratory.

4.4. Limitations and Future Research Directions

This study has three main limitations. First, gravel grain-size measurements were derived from two-dimensional images, which represent the exposed particle surfaces and may be affected by particle overlap, burial, and orientation. Although image processing and independent reprocessing were used to improve measurement consistency, uncertainties associated with two-dimensional representation remain. Second, the study included 15 sampling sites, with uneven representation across the upstream, midstream, and downstream basin zones (4, 8, and 3 sites, respectively). This sampling structure limits the statistical power of regional comparisons and the spatial representativeness of the findings. Third, flow velocity and water depth were measured during individual field surveys and reflect local hydraulic conditions at the time of sampling rather than long-term hydrological variability. Consequently, their relationships with gravel grain-size characteristics should be interpreted as observational associations.

Future research should address these limitations through corresponding methodological improvements. Three-dimensional reconstruction techniques, such as structure-from-motion photogrammetry, could improve the characterization of particle geometry and reduce uncertainties associated with two-dimensional measurements. Increasing the number of sampling sites and improving their spatial distribution would strengthen regional comparisons and help evaluate the consistency of the observed grain-size and multifractal patterns. Repeated hydraulic measurements across different seasons and flow conditions, combined with sediment transport observations, would provide a stronger basis for examining the relationships between hydrological processes and gravel grain-size distributions. These improvements would support a more comprehensive assessment of sediment variability in the Chishui River Basin and comparable river systems.

5. Conclusions

This study combined conventional grain-size statistics with multifractal analysis of high-resolution quadrat imagery of surface gravel from 15 sampling sites in the Chishui River Basin, a representative karst–clastic rock composite watershed in Southwest China, to examine spatial grain-size variability and its multiscale structural characteristics.

(1) Gravel in riparian zones showed substantial site-to-site variability across the Chishui River Basin, but no significant upstream–midstream–downstream zonation was detected. Gravel sizes ranged from 0.07 to 141.07 cm, and individual sites differed considerably in fine-, medium-, and coarse-gravel contents, mean grain size, D_{50}, standard deviation, and CV. In contrast, conventional grain-size descriptors showed no significant differences among the upstream, midstream, and downstream zones. Cumulative frequency distributions also showed that relatively fine-grained and coarse-tailed sites could occur within the same zone. Gravel grain-size variation across the basin therefore cannot be described simply as continuous downstream fining, but is instead characterized by substantial site-to-site variability.

(2) Sampling sites across the Chishui River Basin exhibited broadly similar generalized-dimension spectrum patterns, although individual multifractal parameters differed in their degree of spatial variation. The D_q–q curves at all 15 sites showed similar inverse-S-shaped trends, reflecting comparable overall patterns in the scale-dependent organization of grain-size probabilities. The information dimension (D_1) and correlation dimension (D_2) showed relatively limited regional variation, and no statistically significant differences in multifractal parameters were detected among the upstream, midstream, and downstream zones. However, ΔD and $\Delta\alpha$ varied considerably among individual sampling sites, whereas Δf remained negative at all sites and exhibited relatively limited variation under the reference moment-order range ($q = -10$ to 10). These

findings indicate that gravel grain-size distributions across the basin exhibit broadly similar multifractal spectrum patterns alongside substantial site-to-site variability in selected spectral parameters.

(3) Conventional grain-size descriptors and multifractal parameters showed partially overlapping and potentially complementary information within the investigated dataset. Among the six selected correlations, SD exhibited a significant negative association with ΔD ($\rho = -0.750$, BH-adjusted $q = 0.013$), indicating that greater absolute grain-size dispersion tended to coincide with a narrower generalized-dimension spectrum across the sampled sites. In contrast, the correlations between D_{50} and ΔD and between CV and Δf did not remain statistically significant after BH correction (both $q = 0.067$), and Δf showed no significant associations with the selected conventional descriptors. These findings suggest that conventional grain-size dispersion and probability-dependent scaling characteristics may capture different aspects of the observed grain-size distributions. However, given the limited number of sampling sites and the site-specific nature of the dataset, these interpretations should be regarded as preliminary and confined to the sampled riparian gravel deposits in the Chishui River Basin. Further investigations across additional sites and hydrological conditions are needed to assess their broader applicability.

Author Contributions: Conceptualization, Y.R.; methodology, Y.R., W.C. and K.C.; investigation, Y.R., K.C., Y.L. and Y.H.; data curation, Y.R.; visualization, Y.R.; writing—original draft preparation, Y.R.; writing—review and editing, Y.R., J.X., Y.W. and J.Z.; supervision, J.X.; project administration, J.X.; funding acquisition, J.X.; resources, J.X. All authors have read and agreed to the published version of the manuscript.

Funding: This research was funded by the Science & Technology Fundamental Resources Investigation Program, grant number 2022FY100400, and the National Natural Science Foundation of China, grant number 42507135.

Institutional Review Board Statement: Not applicable. The study involved field observations of gravel sediments and did not involve humans or animals.

Informed Consent Statement: Not applicable.

Data Availability Statement: The data supporting the findings of this study are available from the corresponding authors upon reasonable request.

Acknowledgments: During the preparation of this manuscript, the authors used ChatGPT-6 for translation and language editing. The authors reviewed and edited the output and take full responsibility for the content of this publication.

Conflicts of Interest: The authors declare no conflicts of interest.

References

1. Cao, L.; Liu, S.; Wang, S.; Cheng, Q.; Fryar, A.E.; Zhang, L.; Zhang, Z.; Yue, F.; Peng, T. Factors controlling discharge-suspended sediment hysteresis in karst basins, southwest China: Implications for sediment management. *J. Hydrol.* **2021**, *594*, 125792. [CrossRef]
2. Li, Z.; Xu, X.; Zhu, J.; Xu, C.; Wang, K. Sediment yield is closely related to lithology and landscape properties in heterogeneous karst watersheds. *J. Hydrol.* **2019**, *568*, 437–446. [CrossRef]
3. Li, Z.; Xu, X.; Zhu, J.; Xu, C.; Wang, K.-L. Effects of lithology and geomorphology on sediment yield in karst mountainous catchments. *Geomorphology* **2019**, *343*, 119–128. [CrossRef]
4. Dingle, E.H.; Kusack, K.M.; Venditti, J.G. The gravel-sand transition and grain size gap in river bed sediments. *Earth-Sci. Rev.* **2021**, *222*, 103838. [CrossRef]
5. Rice, S.; Church, M. Grain size along two gravel-bed rivers: Statistical variation, spatial pattern and sedimentary links. *Earth Surf. Processes Landf.* **1998**, *23*, 345–363. [CrossRef]

6. Li, S.; Gao, R.; Huang, M.; Yang, L.; Yu, H.; Yu, C.; Tian, X.; Li, J.; Lin, Y. Multifractal Features of Particle-Size Distribution and Their Relationships With Soil Erosion Resistance Under Different Vegetation Types in Debris Flow Basin. *Front. Earth Sci.* **2022**, *10*, 927862. [CrossRef]
7. Sun, Z.; Gao, Z.; Wang, Y.; Liu, G. Assessing the impact of retrogressive thaw slump on soil structure by analyzing the multifractal characteristics of soil particle size distribution on the Qinghai–Tibet Plateau. *Catena* **2024**, *247*, 108472. [CrossRef]
8. Wang, Y.; He, Y.; Zhan, J.; Li, Z. Identification of soil particle size distribution in different sedimentary environments at river basin scale by fractal dimension. *Sci. Rep.* **2022**, *12*, 10960. [CrossRef] [PubMed]
9. Mandelbrot, B.B. The Fractal Geometry of Nature. *Am. J. Phys.* **1983**, *51*, 286. [CrossRef]
10. Posadas, A.N.D.; Giménez, D.; Bittelli, M.; Vaz, C.M.P.; Flury, M. Multifractal Characterization of Soil Particle-Size Distributions. *Soil Sci. Soc. Am. J.* **2001**, *65*, 1361–1367. [CrossRef]
11. Wang, X.; Sun, L.; Zhao, N.; Li, W.; Wei, X.; Niu, B. Multifractal dimensions of soil particle size distribution reveal the erodibility and fertility of alpine grassland soils in the Northern Tibet Plateau. *J. Environ. Manag.* **2022**, *315*, 115145. [CrossRef] [PubMed]
12. Li, J.; He, X.; Wei, J.; Bao, Y.; Tang, Q.; Nambajimana, J.d.D.; Nsabimana, G.; Khurram, D. Multifractal features of the particle-size distribution of suspended sediment in the Three Gorges Reservoir, China. *Int. J. Sediment Res.* **2021**, *36*, 489–500. [CrossRef]
13. Carrivick, J.L.; Smith, M.W. Fluvial and aquatic applications of Structure from Motion photogrammetry and unmanned aerial vehicle/drone technology. *Wiley Interdiscip. Rev. Water* **2019**, *6*, e1328. [CrossRef]
14. Piégay, H.; Arnaud, F.; Belletti, B.; Bertrand, M.; Bizzi, S.; Carbonneau, P.; Dufour, S.; Liébault, F.; Ruiz-Villanueva, V.; Slater, L. Remotely sensed rivers in the Anthropocene: State of the art and prospects. *Earth Surf. Processes Landf.* **2020**, *45*, 157–188. [CrossRef]
15. Lang, N.; Irniger, A.; Rozniak, A.; Hunziker, R.; Wegner, J. GRAINet: Mapping grain size distributions in river beds from UAV images with convolutional neural networks. *Hydrol. Earth Syst. Sci.* **2021**, *25*, 2567–2597. [CrossRef]
16. Graham, D.J.; Rice, S.P.; Reid, I. A transferable method for the automated grain sizing of river gravels. *Water Resour. Res.* **2005**, *41*, W07020. [CrossRef]
17. Feeney, C.J.; Chiverrell, R.C.; Smith, H.G.; Hooke, J.M.; Cooper, J.R. Modelling the decadal dynamics of reach-scale river channel evolution and floodplain turnover in CAESAR-Lisflood. *Earth Surf. Processes Landf.* **2020**, *45*, 1273–1291. [CrossRef]
18. Miazza, R.; Pascal, I.; Ancey, C. Automated grain sizing from uncrewed aerial vehicles imagery of a gravel-bed river: Benchmarking of three object-based methods. *Earth Surf. Processes Landf.* **2024**, *49*, 1503–1514. [CrossRef]
19. Wong, T.; Khanal, S.; Zhao, K.; Lyon, S.W. Grain size estimation in fluvial gravel bars using uncrewed aerial vehicles: A comparison between methods based on imagery and topography. *Earth Surf. Processes Landf.* **2024**, *49*, 374–392. [CrossRef]
20. Buscombe, D. SediNet: A configurable deep learning model for mixed qualitative and quantitative optical granulometry. *Earth Surf. Processes Landf.* **2020**, *45*, 638–651. [CrossRef]
21. Carbonneau, P.E.; Lane, S.N.; Bergeron, N.E. Catchment-scale mapping of surface grain size in gravel bed rivers using airborne digital imagery. *Water Resour. Res.* **2004**, *40*, W07202. [CrossRef]
22. Chardon, V.; Schmitt, L.; Piégay, H.; Lague, D. Use of terrestrial photosieving and airborne topographic LiDAR to assess bed grain size in large rivers: A study on the Rhine River. *Earth Surf. Processes Landf.* **2020**, *45*, 2314–2330. [CrossRef]
23. Spearman, C. The Proof and Measurement of Association between Two Things. *Am. J. Psychol.* **1904**, *15*, 72–101. [CrossRef] [PubMed]
24. Benjamini, Y.; Hochberg, Y. Controlling the False Discovery Rate: A Practical and Powerful Approach to Multiple Testing. *J. R. Stat. Soc. Ser. B* **1995**, *57*, 289–300. [CrossRef]
25. Sklar, L.S.; Riebe, C.S.; Genetti, J.; Leclere, S.; Lukens, C.E. Downvalley fining of hillslope sediment in an alpine catchment: Implications for downstream fining of sediment flux in mountain rivers. *Earth Surf. Processes Landf.* **2020**, *45*, 1828–1845. [CrossRef]
26. Ma, Z.; Ma, Y.; Zhao, X.; Zhang, J.; Zhang, H. Downstream fining of fluvial gravels along the eastern Tibetan Plateau rivers. *Earth Surf. Processes Landf.* **2025**, *50*, 70016. [CrossRef]
27. Cook, K.L.; Turowski, J.M.; Hovius, N. Width control on event-scale deposition and evacuation of sediment in bedrock-confined channels. *Earth Surf. Processes Landf.* **2020**, *45*, 3702–3713. [CrossRef]
28. Savi, S.; Tofelde, S.; Wickert, A.; Bufe, A.; Schildgen, T.; Strecker, M. Interactions between main channels and tributary alluvial fans: Channel adjustments and sediment-signal propagation. *Earth Surf. Dyn.* **2020**, *8*, 303–322. [CrossRef]
29. Xie, J.; Coulthard, T.J.; Cao, J.; Wu, J.; Wang, M. How does landslide debris grain size control sediment transport and dynamics? *Geomorphology* **2024**, *451*, 109050. [CrossRef]
30. Li, Z.; Xu, X.; Wang, K. Effects of distribution patterns of karst landscapes on runoff and sediment yield in karst watersheds. *Catena* **2023**, *223*, 106947. [CrossRef]

Disclaimer/Publisher's Note: The statements, opinions and data contained in all publications are solely those of the individual author(s) and contributor(s) and not of MDPI and/or the editor(s). MDPI and/or the editor(s) disclaim responsibility for any injury to people or property resulting from any ideas, methods, instructions or products referred to in the content.